Chapter 3

STRONG ELECTRIC FIELD EFFECT ON SOME NEMATIC LIQUID CRYSTALS

3.1 Introduction

In the previous chapter we have described an experimental technique which allows us to measure the local temperature of the sample under the application of a strong electric field.. We have also described setups for electrical impedance measurement and optical studies. In this chapter we present experimental results obtained using these techniques to study the electric field effect on the nematic-isotropic phase transition in a few compounds. First we will discuss the theoretical background to this problem on the basis of a phenomenological Landau model.

3.2 Theoretical Background

3.2.1 Landau Theory of Phase Transitions

The Landau theory is a phenomenological theory initially developed to describe phase transitions of the second kind. It is assumed that near a second order phase transition point, the free energy density F can be expanded in powers of the order parameter (S) characterising the phase with the lower symmetry [45]. In the absence of any external field the expansion is as follows:

$$F(p, T, S) = F_o + \frac{A}{2}S^2 + \frac{B}{3}S^3 + \frac{C}{4}S^4...$$ (3.1)

where F_o is the free energy density when $S = 0$. The dependence of the order parameter near the phase transition point is then determined by minimising Equation **3.1** with respect to S. The term linear in S is absent to ensure the stability of the higher symmetry phase. It can be non zero when an external symmetry breaking field is introduced. $A > 0$ ensures that $S = 0$ corresponds to a minimum in F for the higher temperature phase and $A < 0$ corresponds to that of $S \neq 0$ for the lower temperature phase.

Landau assumed that $A = a(T - T^*)$ where T^* is the transition temperature. B and C are normally assumed not to change with temperature. For a system in which the free energy density is independent of the sign of S i.e. $F(S) = F(-S)$ the cubic and higher odd powers of S are not allowed as for example, in a ferromagnetic system. In this case for $B = 0$, and for $C > 0$ a second order phase transition takes place between the states $S = 0$ and $S \neq 0$ at $T = T^*$. Minimising Equation *3.1* with respect to S the temperature dependence of the order parameter

is found to be

$$S = \left(\frac{a(T - T^*)}{C}\right)^{\frac{1}{2}}.$$

(3.2)

The above argument has been extended to describe weakly first order phase transitions. One way of obtaining a first order transition is to have a third order term. If the symmetry of the system prevents the presence of a third order term (i.e. $B = 0$) then a first order transition can be obtained by having $C < 0$. In that case a stabilising sixth order term with coefficient $E > 0$ is required.

3.2.2 Landau-de Gennes Theory for the Nematic-Isotropic Phase Transition

The Landau theory for the nematic-isotropic phase transition has been reviewed in detail by Gramsbergan et *al* [25]. In the nematic phase the orientational order parameter (as described in Chapter 1) is defined as

$$S = \frac{1}{2} < 3\cos^2\theta - 1 >$$

(3.3)

which is essentially a second rank tensor. As such, it can be seen that S can take values between 1 and $-\frac{1}{2}$. These two extreme values of S describe two distinct physical situations. The first one corresponds to $\theta = 0$ and the latter to $\theta = \frac{\pi}{2}$. In general positive and negative S arise from different distribution functions, hence $F(S) \neq F(-S)$. Thus the free energy density expansion for the nematic phase should include odd powers of S.

The free energy density for the nematic phase is hence written as

$$F(p, T, S) = F_o + \frac{a(T - T^*)}{2}S^2 - \frac{B}{3}S^3 + \frac{C}{4}S^4$$

(3.4)

where T^* is the temperature below which the isotropic phase cannot be supercooled. The cubic term is assumed to be negative to get positive values of S in the nematic phase for positive B. Minimising Equation 3.4 with respect to S we get three solutions

$$S = 0$$

(3.5)

$$S_{\pm} = \frac{B}{2C}\left[1 \pm \left(1 - \frac{4Ca(T - T^*)}{B^2}\right)^{\frac{1}{2}}\right].$$

(3.6)

$S = 0$ corresponds to the isotropic phase. S_- corresponds to a maximum in the free energy density and is not an acceptable solution. S_+ corresponds to a minimum in the free energy density and hence S_+ is a stable solution. We calculate the transition temperature T_{NI} by equating the free energy density of the nematic phase to that of the isotropic phase i.e. $F(p, T, S) = F_o$.

$$\frac{a(T_{NI} - T^*)}{2}S_{NI}^2 - \frac{B}{3}S_{NI}^3 + \frac{C}{4}S_{NI}^4 = 0$$

(3.7)

where S_{NI} is the order parameter at the transition point. The equilibrium condition yields

$$a(T_{NI} - T^*)S_{NI} - BS_{NI}^2 + CS_{NI}^3 = 0.$$

(3.8)

From Equations 3.7 and **3.8** we get

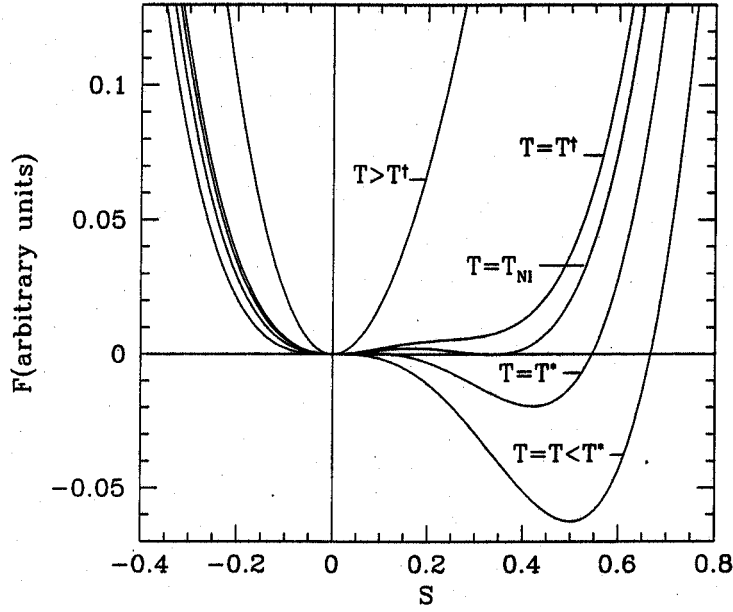$$\frac{BS_{NI}^3}{3} \cdot \frac{CS_{NI}^4}{2}$$

(3.9)

Figure 3.1: Variation of the free energy density as a function of order parameter at various temperatures near the nematic-isotropic transition point.

$$S_{NI} = \frac{2B}{3C} \quad , \quad T_{NI} = T^* + \frac{2B^2}{9aC}. \tag{3.10}$$

Equation 3.6 has solutions only when $1 - \frac{4Ca(T-T^*)}{B^2} > 0$, leading to an upper temperature limit above which the nematic phase cannot exist. This temperature $T^\dagger$ is

$$T^\dagger = T^* + \frac{B^2}{4Ca}. \tag{3.11}$$

Figure 3.1 shows the variation of the free energy density as a function of order parameter for various temperatures.

For $T > T^\dagger$ there is only one minimum for the free energy corresponding to $S = 0$, i.e. the isotropic phase. At $T = T^\dagger$, there is an inflection point in the free energy density curve. For $T_{NI} < T < T^\dagger$ there are two minima for the free energy density one corresponding to the isotropic phase (i.e. the absolute minimum) and the other corresponding to the superheated nematic phase (i.e. a local minimum). At $T = T_{NI}$ there are two equal minima and hence a first order phase transition takes place from $S = 0$ to $S = S_{NI}$. For $T^* < T < T_{NI}$ there are again two minima, the absolute minimum corresponding to a nonzero S whereas a local minimum corresponds to $S = 0$. This allows for the supercooling of the isotropic phase. At $T = T^*$ there is only one minimum for the free energy density corresponding to $S > S_{NI}$ and an inflection point at $S = 0$. Below T^* the isotropic phase cannot be further supercooled as there is only one minimum in the free energy density corresponding to $S > S_{NI}$.

Thus from the presence of a nonzero third order term the nematic-isotropic transition is first order in nature. Typically, the order parameter at the transition point $S_{NI} \sim 0.3$ which in principle is not very small. However from the thermodynamic point of view the nematic-isotropic
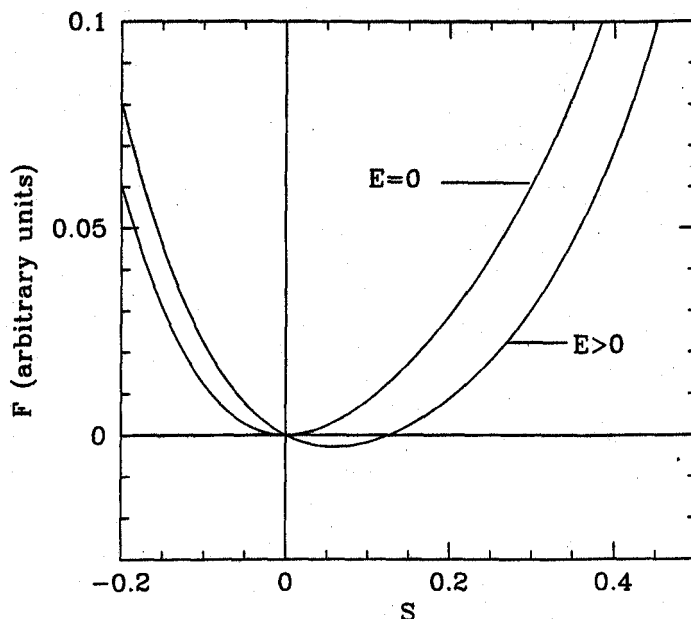
Figure 3.2: Variation of the free energy density as a function of the order parameter in the presence and absence of an electric field for $T > T^{\dagger}$.

phase transition is a *weakly* first order phase transition. The heat of transition of the nematic-isotropic phase transition is very small ($-$ **0.2kcal/mol**) in comparison to the crystal-liquid crystal melting transition ($\sim$ **5kcal/mol**).

3.2.3   N-I Transition in the Presence of an Electric field

As explained in Chapter 2 in the presence of an external field, a linear term in S has to be included in the Landau free energy density. Following the argument described in Section 3.2.1, in the presence of a linear term in S, the isotropic phase cannot exist as now the free energy density will be a minimum only for a finite value of **S.** The free energy density for the nematic phase in the presence of an electric field is

$$F(p, T, S) = F_o(p, T) - hS + \frac{A}{2}S^2 - \frac{1}{3}BS^3 + \frac{1}{4}CS^4 \tag{3.12}$$

where $h = \frac{1}{12\pi}\Delta\epsilon_o E^2 = -\mu_e E^2$. Minimising Equation 3.12 with respect to S gives

$$a(T - T^*) = h/S + BS - CS^2. \tag{3.13}$$

This shows that when the field is switched on, a given value of S occurs at a higher temperature. Figure 3.2 shows the variation of the free energy density at zero field and in the presence of a finite field for $T > T^{\dagger}$, and for a system with $\epsilon_a > 0$. It is seen that for a finite value of E the free energy density is minimised for a nonzero value of S. Figure 3.3 shows the theoretical variation of the order parameter as a function of reduced temperature at different fields. As described in Chapter 2 beyond a critical field there is a continuous evolution of the order parameter as the temperature is varied.
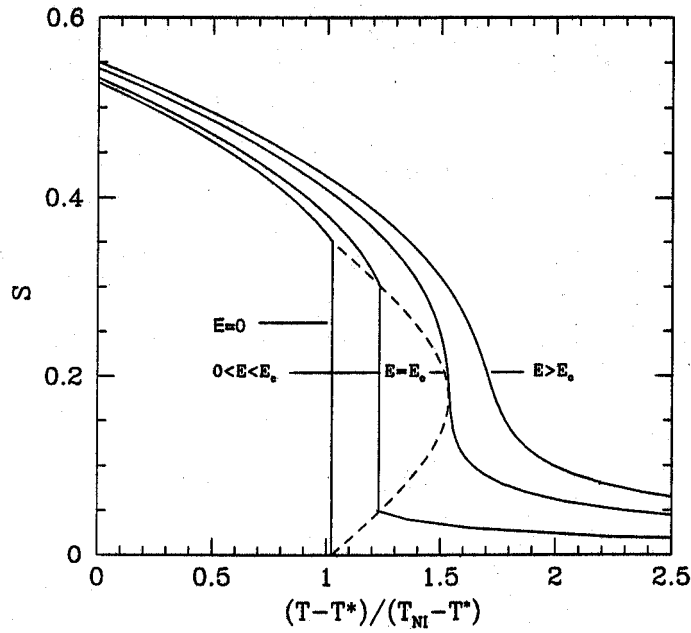
Figure **3.3:** Theoretical variation of the order parameter as a function of reduced temperature at different electric fields. The dashed line is the coexistence curve.

At the critical point $F' = F'' = 0$. Differentiating Equation **3.12** twice with respect to S and equating the results to 0, at the critical point the following equations are obtained

$$S_c = \frac{B}{3C}$$

$$T_c = T^* + \frac{B^2}{3aC}$$

$$E_c^2 = -\frac{BS_c^2}{3\mu_e}$$

$$(3.14)$$

where S_c and T_c are the coordinates of the critical point on the temperature order parameter phase diagram at the critical field E_c.

For a system with negative dielectric anisotropy the situation is slightly different. When $\epsilon_a < 0$ the director aligns perpendicular to the field. In the isotropic phase this would lead to a paranematic phase with orientational order around the field direction but with $< \theta >$ tending towards 90°. This corresponds to a phase with negative order parameter (N_{U-}). In the nematic phase, let us assume that the sample is taken between two **glass** plates which are treated for homogeneous alignment of the director, along a direction parallel to the glass plates. When an electric field is applied perpendicular to the glass plates an additional orientational order sets in around the field direction. This field suppresses the thermal fluctuations of the director in the plane containing the electric field and the director. In the presence of an electric field the nematic phase has orientational order around two directions vk. around E and parallel to the glass plates, and is hence biaxial (N_B) in nature. As discussed by **Gramsbergan** et al [25], for low fields a first order phase transition occurs from the field induced uniaxial phase to the biaxial phase as the temperature is reduced. Beyond a certain field this first order phase transition
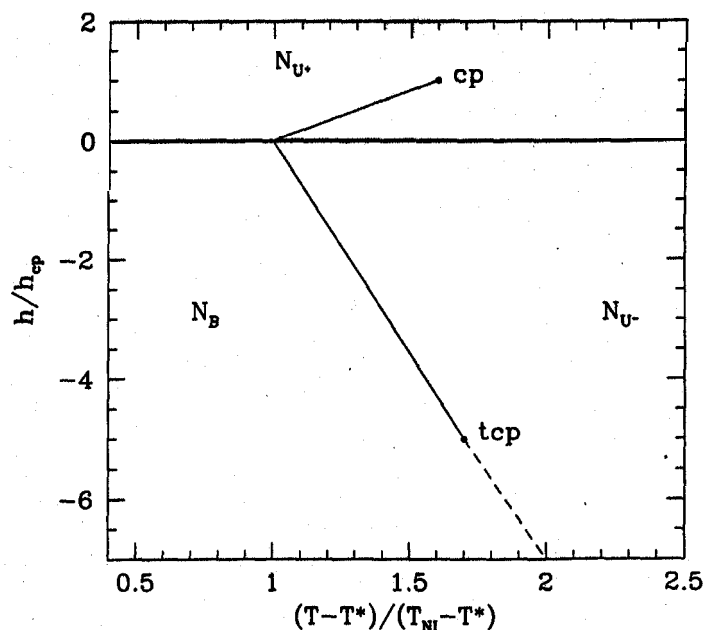
Figure **3.4:** T,h phase diagram of a nematic. Thick solid lines are first order transitions, dashed lines second order : cp and tcp are critical and tricritical points. Reproduced from Reference [25].

changes over to a second order phase transition. This point on the phase diagram is a tricritical point. Figure **3.4** shows the phase diagrams for nematic liquid crystals with both positive and negative dielectric anisotropies as functions of reduced temperature and field.

In Section **3.3.1** we present experimental results which describe the effect of an electric field on the nematic-paranematic phase transition using impedance measurements on two nematic liquid crystals with positive dielectric anisotropy. In Section **3.3.2** we present experimental results on the effect of a strong electric field on a nematogen with negative dielectric anisotropy using optical measurements.

3.3   **Experimental Results and Discussion**

We have studied the effect of strong electric fields in the following compounds using the impedance measurements: 4'-n-pentyl-4cyanobiphenyl (**5CB**) and **4'-n-octyloxy-Pcyanobiphenyl** (8OCB). The chemical structures of these compounds and their transition temperatures are shown in Figure 3.5. These compounds were obtained from Roche and were used without further purification. We chose these compounds as they have large positive dielectric anisotropies. Further they have relatively low N-I transition temperatures. All the compounds are chemically stable.

The field effect on the orientational order parameter in **5CB** has been studied by Lelidis et al [37, 38]. As described in Chapter 2 they were able to probe the critical region. They also measured the linear and quadratic variation of the order parameter due to the quenching of the thermal fluctuations and the Kerr effect in the nematic phase.

We have also studied the effect of a strong electric field on **4-methoxyphenyl-trans-4-** pentylcyclohexylcarboxylate (**S1495**). We chose this compound as it had the largest negative dielectric anisotropy ($\sim$ **−1.3**) amongst the compounds available to us. The chemical structure
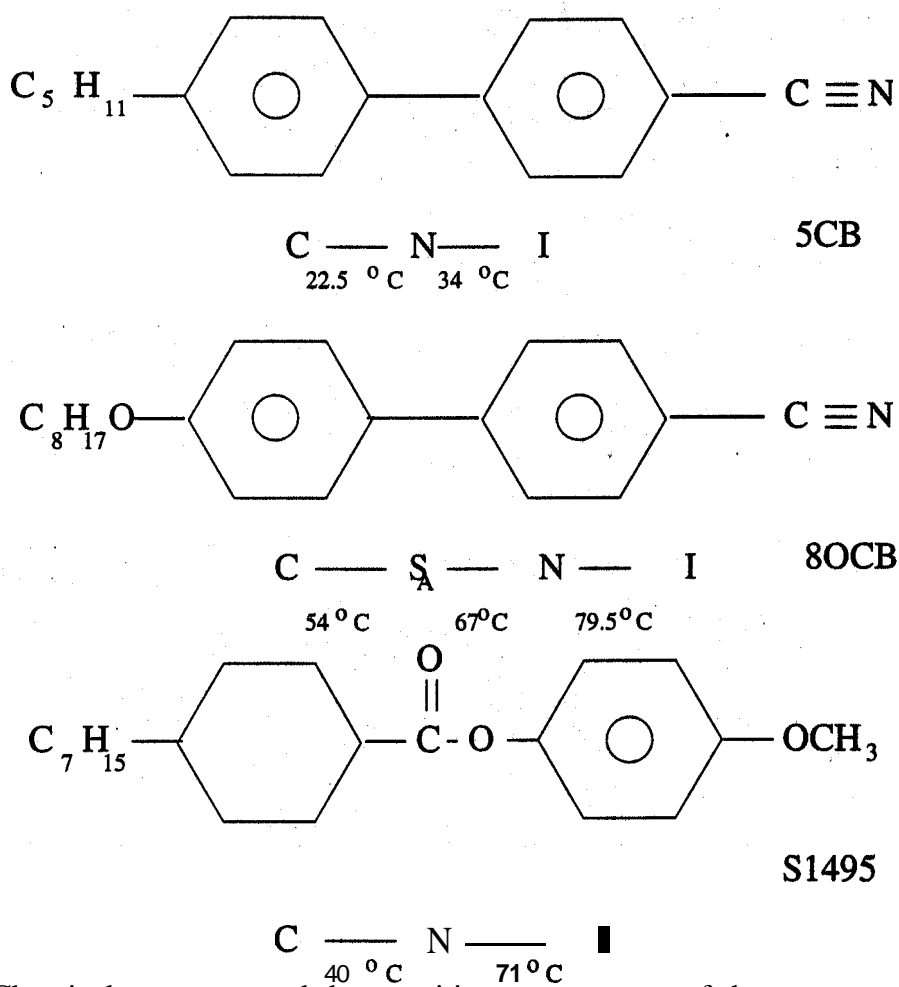
$$C_5 H_{11} - \bigcirc\bigcirc - C \equiv N$$

$$C \underset{22.5\ ^\circ C}{\rule{2cm}{0.4pt}} N \underset{34\ ^\circ C}{\rule{1.5cm}{0.4pt}} I \qquad \text{5CB}$$

$$C_8 H_{17} O - \bigcirc\bigcirc - C \equiv N$$

$$C \underset{54\ ^\circ C}{\rule{1.5cm}{0.4pt}} S_A \underset{67^\circ C}{\rule{1.5cm}{0.4pt}} N \underset{79.5^\circ C}{\rule{1.5cm}{0.4pt}} I \qquad \text{8OCB}$$

$$C_7 H_{15} - \bigcirc - \overset{\overset{\textstyle O}{\|}}{C} - O - \bigcirc - OCH_3$$

S1495

$$C \underset{40\ ^\circ C}{\rule{1.5cm}{0.4pt}} N \underset{71\ ^\circ C}{\rule{1.5cm}{0.4pt}} \blacksquare$$

Figure 3.5: Chemical structures and the transition temperatures of the compounds used in the experimental studies in this chapter.

and the transition temperatures of this compound are also shown in Figure 3.5. This compound was obtained from **Merck** and was used without further purification. We have used **optical** measurements in this case. As the dielectric **anisotropy** is relatively small we were not able to observe a very pronounced effect in this sample.

3.3.1 Strong Electric Field Effect on the N-I transition in Two Nematogens with Positive Dielectric Anisotropy

For these experiments we used the initial setup which is described in Chapter 2 (Figure 2.19). In these first experiments we used cells with the simpler electrode configuration **i.e.** without the guard ring (Figure 2.2). The top plate was aluminium coated (Figure 2.4). We used 19 μm spacers and we have assumed that the thickness of the cell is equal to the thickness of the mylar spacer. At any given Mettler temperature, a few preset sinusoidal voltages were applied to the cell. The signal is measured on the **amplitude-phase** (R-8) mode of the lock-in-amplifier. In this mode the phase is adjusted for maximum R. When the ratio of the out of phase component (the component of the signal at **90°** phase with respect to that for maximum R) to the **inphase** component (R) is less than a preset value ($\sim$ 1 to 2%) the electrical parameters of the cell **as** well as its local temperature are measured. At higher voltages, the temperature of the cell is higher. All the measurements were made while cooling the sample from the isotropic phase. A flow chart of the program is shown in Figure 3.6.

Figure 3.7 shows the variation of the dielectric constant of an 80CB sample of thickness $\sim$ 19 μm, with an AC voltage of $\sim$ 334 V and frequency of f = 6720 Hz applied to it, as a function of the set *Mettler temperature.* Figure 3.8 shows the **variation** of the same dielectric data as a function of the *local* temperature measured by the nickel resistance thermometer. It can be seen that there is a difference in the actual shape of the two curves. This shape change is due to the variation of the local heating of the sample as a function of the temperature when a large voltage is applied to the cell. The applied voltage is slightly higher than the critical voltage which has been calculated to be $\sim$ 300 V. It is seen from Figure 3.9 that the variation of the heating effect at a specific voltage is highly sensitive to the sample temperature especially around the critical region. In this range there is a decrease in the electrical resistance of the sample which is accompanied by an increase in the local heating of the sample. This point will be discussed in more detail in Chapter 5. So, it is not sufficient to apply a constant voltage to the sample and assume that the local heating is independent of the temperature of the sample as was done by Nicastro and Keyes [36].

INPUT

TEMPERATURE -T
START TEMPERATURE -ST   ELECTRICAL SIGNAL -V �
END TEMPERATURE -ET   NICKEL RESISTANCE - R
TEMPERATURE STEP -TS
WAIT TIME -T1,T2   OPTICAL SIGNAL -OS
START VOLTAGE -VS
END VOLTAGE-VE
NUMBER OF VOLTAGE POINTS -NV
VOLTAGE STEP -DV=(VE-VS)/NV
POST EXPERIMENT TEMPERATURE-PET
RATIO OF OUT OF PHASE VOLTAGE TO IN PHASE VOLTAGE-RP
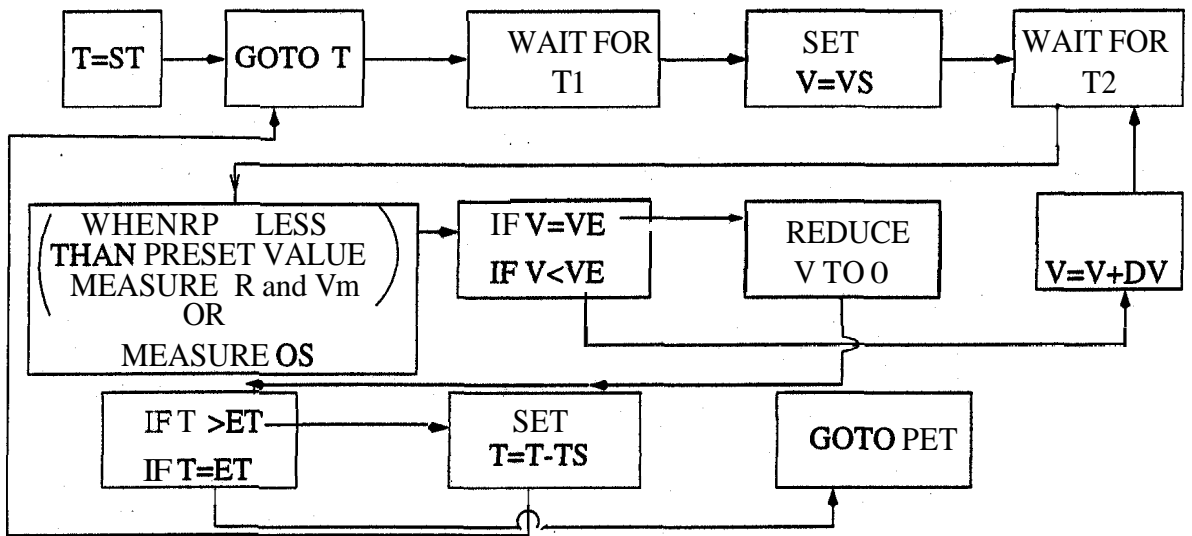
Figure 3.6: Flow chart for the programme used to conduct the experiments.
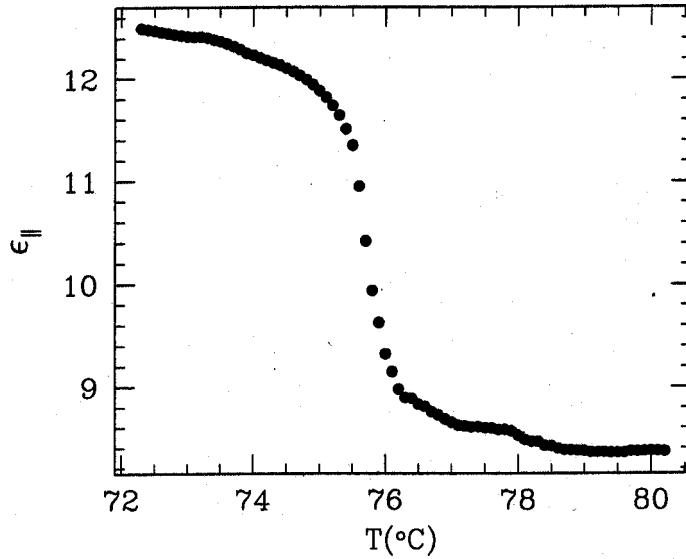
Figure 3.7: Variation of the dielectric constant of an 80 CB sample 'as a function of the set Mettler temperature. V=334.5 V and f=6720 Hz. The thickness of the cell is d = 19 μm.
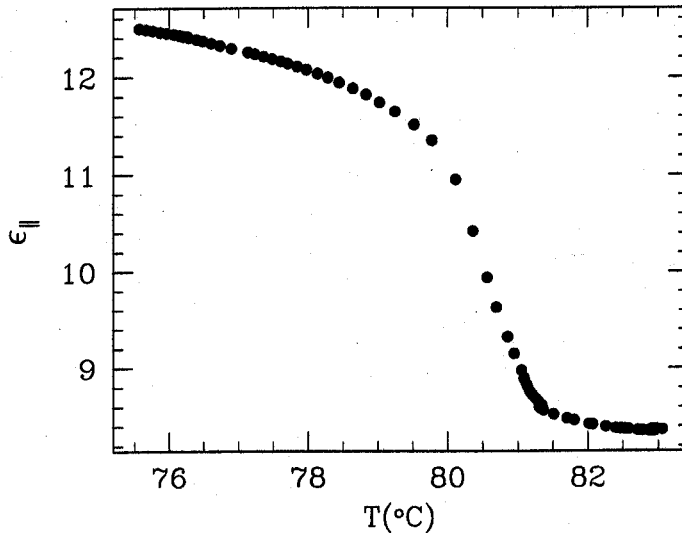
Figure 3.8: Same data as shown in Figure 3.7, but now plotted as a function of the local temperature measured by the nickel resistance thermometer.
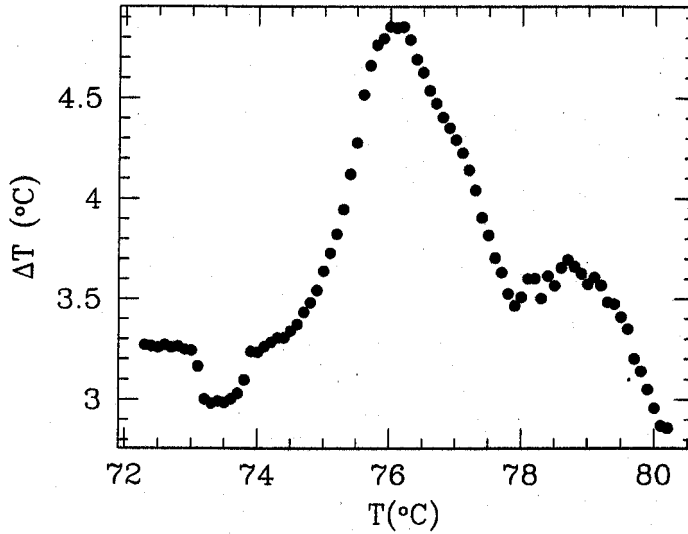
Figure **3.9:** Difference between the local temperature and the set temperature of the Mettler hot stage plotted as a function of the local temperature calculated from the experimental data shown in Figures **3.7** and 3.8.

3.3.1.1 Analysis

As shown in Equations **1.12** and **1.15** according to the Maier and Meier theory

$$\epsilon_{\parallel} = 1 + 4\pi \frac{N_A \rho h F}{M} \left\{ \bar{\alpha} + \frac{2}{3} \Delta \alpha S + \frac{F \mu^2}{3 k_B T} \left[1 - \left(1 - 3 \cos^2 \beta \right) S \right] \right\} \tag{3.15}$$

$$\bar{\epsilon} = 1 + 4\pi \frac{N_A \rho h F}{M} \left(\bar{\alpha} + \frac{F \mu^2}{3 k_B T} \right) \tag{3.16}$$

Hence the relationship between $\epsilon_{\parallel}$ and the orientational order parameter S can be approximately written in the form

$$\epsilon_{\parallel} = \bar{\epsilon} + \frac{2}{3} \Delta \epsilon_o S \tag{3.17}$$

where $\Delta \epsilon_o$ is the anisotropy for a medium with **S=1** and $\bar{\epsilon}$ is the average dielectric constant. It can be seen from Equations **3.15** and **3.16** that both $\bar{\epsilon}$ and $\epsilon_{\parallel}$ are temperature dependent and in principle $\Delta \epsilon_o$ will be temperature dependent. In the experiments to be described in the coming sections we have made measurements over a small temperature range, **and** for simplicity we have ignored this temperature dependence. It is well known that in materials with highly polar end groups, the antiparallel near neighbour correlations lead to a slightly lower value of $\bar{\epsilon}$ in the nematic phase compared to that of the isotropic phase at T_{NI} [16]. We have taken $\bar{\epsilon}$ to be **1.5%** smaller than the value measured in the isotropic phase at low applied fields to take account of this fact. We have used the orientational order parameter measured by an optical technique [46] at $T_{NI} - 2°$C to evaluate $\Delta \epsilon_o$. The nematic order parameter variation with field can now be compared with the prediction of the Landau theory discussed in Section **3.2.3.**
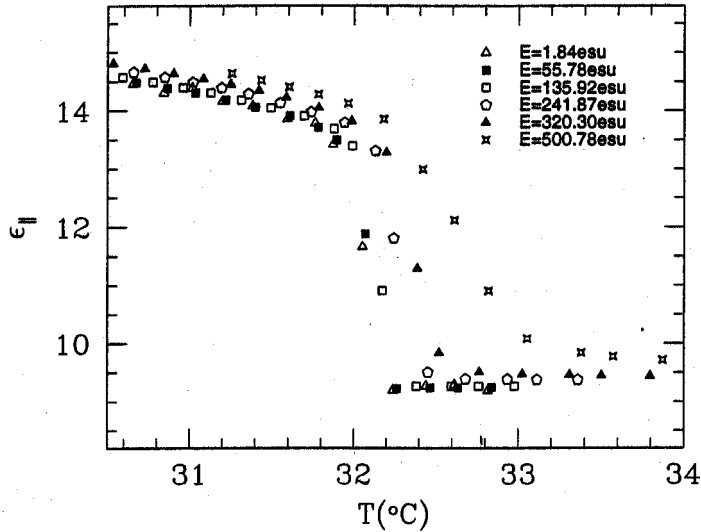
Figure **3.10:** Dielectric constant of **5CB** as a function of temperature at different fields. Thickness of the cell d = **19** μm. Frequency of the applied voltage f =**2317** Hz.

3.3.1.2 Measurements on 5CB

$\epsilon_{\parallel}$ is shown as a function of the local temperature for various values of the applied field in a **5CB** sample in Figure **3.10.** $\Delta\epsilon_o$ (= **18.1**) is calculated following the procedure described in Section **3.3.1.1.** The order parameter is calculated using Equation **3.17** (Figure **3.11**). As the **N-I** transition has a first order character the **4-parameter** Landau theory can be expected to be inadequate especially at temperatures below T_{NI}. Hence we have used only the data measured close to this temperature and for electric fields close to the critical field in the analysis using Equation **3.13.** Figure **3.12** shows the experimental points as well as the calculated variation. The best overall fit was obtained for the following parameters:

T_{NI} - T*= **1.3** $\pm$ **0.06** in °C

$B/a =$ **11.0** $\pm$ **0.1** in cgs units

$C/a =$ **21.4** $\pm$ **0.15** in cgs units

$a =$ (**1.0** $\pm$ **0.04**)$\times$ **10**^{6} in cgs units

$E_c \simeq$ **440** esu.

These parameters are broadly consistent with the values given by Lelidis and Durand [38]. We should note that the calculated temperature variation of **S** in the nematic phase is steeper than that of the experimental data. It is known from a number of earlier studies on nematic liquid crystals that the order parameter variation is less rapid than that predicted by the mean field theory. Often this is assumed to be due to a tricritical rather than a critical behaviour [25].

3.3.1.3 Measurements on 8OCB

The measured values of the dielectric constants of 80CB are shown in Figure **3.13.** $\Delta\epsilon_o =$ **13.0.** The order parameter is calculated as described in Section **3.3.1.1** (here we have taken the order parameter measurements from Reference [44]). Figure **3.14** shows the variation of the order
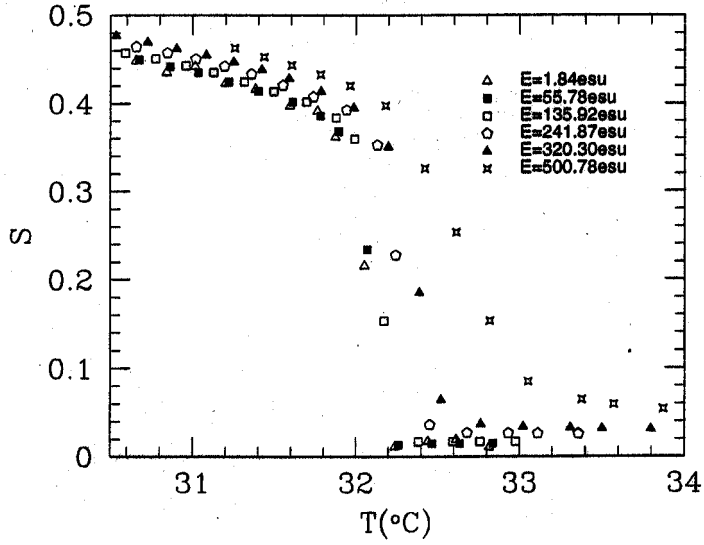
Figure **3.11:** Orientational order parameter *S* of 5CB calculated from the data shown in Figure **3.10.**
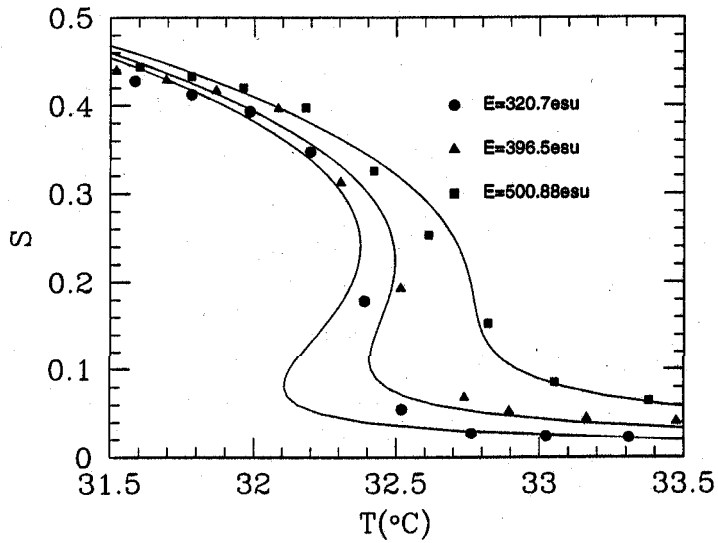

Figure **3.12:** Orientational order parameter of 5CB **as** a function of temperature at different fields. Solid curves show the theoretical variation given by the Landau theory. Same sample **as** described in Figure **3.10.**
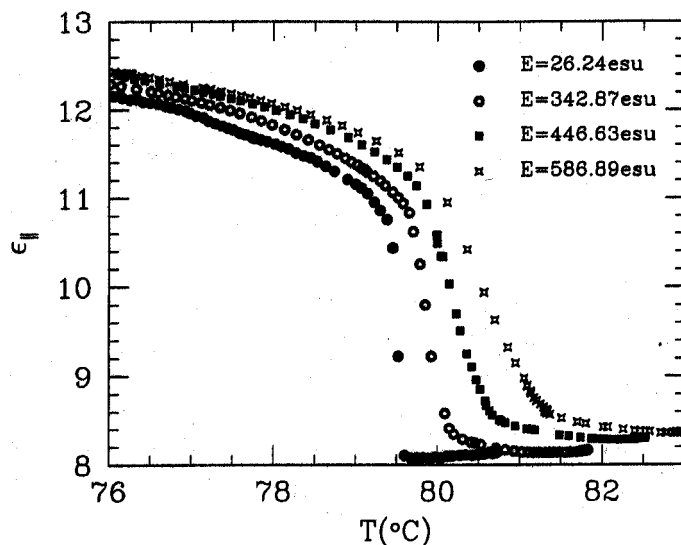
Figure 3.13: Dielectric constant of 80CB as a function of temperature at different fields. Thickness of the cell d $=$ 19 μm. Frequency of the applied voltage f=6170Hz.

parameter of 80CB as a function of temperature at different fields. The variations of S for different fields given by the Landau model are shown in Figure 3.15 for temperatures close to the N-I transition and the critical field. The Landau parameters in this case are listed below:

T_{NI} - T* = 1.2 $\pm$ 0.2 in °C

B/a = 13.5 in cgs units

C/a = 29.2 $\pm$ 0.2 in cgs units

a = (0.87$\pm$0.1) x 10^6 in cgs units

E_c $\simeq$ 540 esu .

The Landau coefficients of 5CB and 80CB are comparable. The value of a in 80CB is $\sim$ 10% less than that in 5CB. E_c is higher in 8OCB than that in 5CB as $\Delta\epsilon_o$ = 13 in 80CB which is considerably smaller than that in 5CB ($\Delta\epsilon_o$ = 18.1).
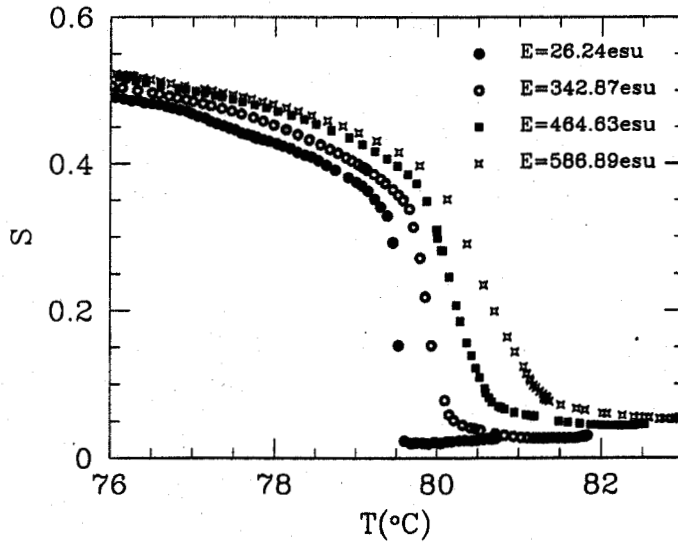
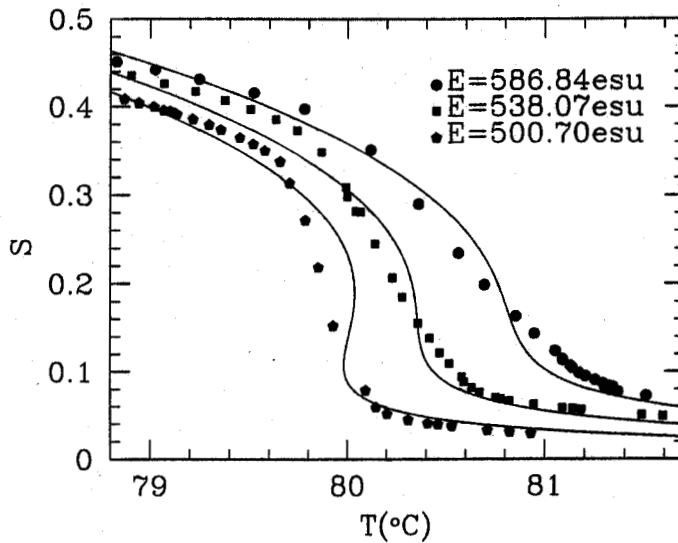Figure **3.14:** Orientational order parameter S for 80CB calculated from the data shown in Figure **3.13.**

Figure **3.15:** Orientational order parameter of **8OCB as** a function of temperature at different fields. Solid curves show the theoretical variation given by the Landau theory. Same sample as described in Figure **3.13.**
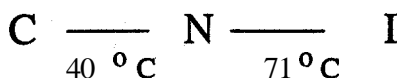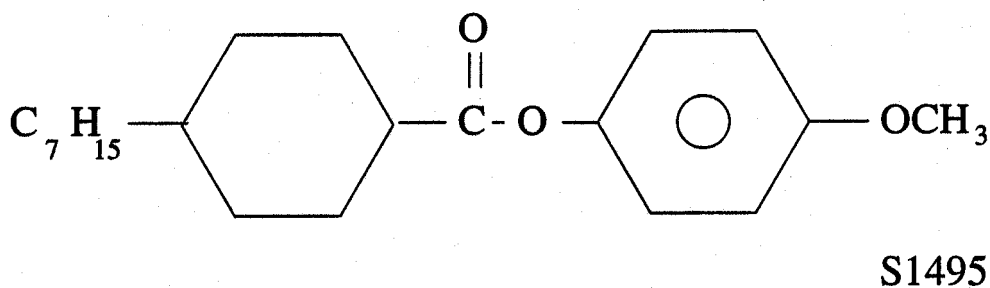
Figure 3.16: Chemical structure and transition temperatures of S1495.

3.3.2 Strong Electric Field Effects on a Nematogen with Negative Dielectric Anisotropy

Electric field effects on nematogens with negative dielectric anisotropy have been reported by Nicastro and Keyes [36] and Rjumtsev et *al* [43]. They have measured the field induced birefringence in some compounds in the isotropic phase. As mentioned previously S1495 is a nematogen with negative dielectric anisotropy. The chemical structure of S1495 and the transition temperatures are shown in Figure 3.16. The nematic phase of this compound supercools to room temperature. In this section we report experimental results on the effect of a strong electric field on the N-I transition in S1495 using optical measurements in the reflection mode of the microscope. We have measured the DC transmitted intensity as a function of temperature at different fields. From these measurements we have calculated the variation of the orientational order parameter.

The sample was taken in a cell, the bottom plate of which is similar to that shown in Figure 2.2. It consists of the nickel resistance thermometer and the electrode without the guard ring. The top plate is a transparent ITO coated glass plate with an electrode pattern etched in it (Figure 2.4). The aluminium electrode reflects the incident light back to the photodiode. Both the plates are treated with SiO_2 (coated in vacuum at a grazing angle of 30°) for homogeneous alignment of the director. The thickness of the cell was controlled by mylar spacers of thickness ~ 12 μm. The optical setup is shown in Figure 2.16. The cell is placed in a Mettler hot stage which itself is kept on the stage of a polarising microscope. The sample is illuminated by a He-Ne laser beam and the director is aligned perpendicular to the direction of light propagation. The experimental procedure is similar to that described in Section 3.3.1. The flow chart of the programme is shown in Figure 3.6 and as mentioned above we have measured a DC optical intensity instead of the electrical parameters of the cell.

When the sample is placed between crossed polarisers the transmitted intensity is given by

$$T = \sin^2 2\psi \frac{(1 - \cos \Delta\phi)}{2} \tag{3.18}$$

ψ (=45 ° in the present case) is the angle between the director and the polariser. $\Delta\phi$ is the phase difference between the ordinary and extraordinary waves and is given by

$$\Delta\phi = \frac{2\pi}{\lambda}(n_e - n_o)2d \tag{3.19}$$

where n_o and n_e are the ordinary and extraordinary refractive indices of the liquid crystal. λ is the wavelength of light used (0.633 μm) and 2d is twice the sample thickness (as the light

beam passes through the sample twice). A minimum and a maximum in the transmitted optical intensity correspond to

$$\Delta\phi = 2n\pi$$

or

$$\Delta\phi = (2n + 1)\pi \tag{3.20}$$

respectively, where n is an integer. Figure 3.17 shows the variation of the transmitted optical intensity as a function of temperature for different applied fields in a small temperature range close to T_{NI}. The frequency of the applied voltage is 15111 Hz. As mentioned in Section 3.2.3 the paranematic phase above the transition temperature is uniaxial with negative order parameter. As we are viewing the sample along the optic axis there is no path difference and the intensity between crossed polarisers is zero.

To calculate the variation of the birefringence with temperatufe in the nematic phase we need to know the value of n given in Equation 3.20. For this purpose we have measured the variation of the optical intensity as a function of temperature at zero field (Figure 3.18) over a wide range of temperatures. From magndtic susceptibility measurements (see Chapter 7) the orientational order parameter at 46.5°C and 68.3°C which correspond to a maximum (from Figure 3.18) and a minimum (from Figure 3.17) in intensity are 0.716 and 0.457 respectively. S is given by

$$S = \frac{\Delta n}{\Delta n_o} \tag{3.21}$$

where An $= n_e - n_o$ and An, is the birefringence for the fully aligned state. Substituting for An in Equation 3.19 at the above stated temperatures and using Equations 3.20 we find that the minimum at T $= 68.3$°C corresponds to n $= 3$. Using this we have calculated $2d\Delta n$ at T $= 68.3$°C and also as a function of temperature (using Equation 3.18) from the data shown in Figure 3.17. Calibrating this data with respect to the order parameter as measured from the magnetic susceptibility at T_{NI} - 1.7°C we evaluate the order parameter as a function of temperature at different fields (Figure 3.19).

We have plotted the transition temperature (T_{NI}) as a function of field (Figure 3.20). We see that there is a large shift in the transition temperature (~ 0.2°C) between the zero field and the E $= 173.61$ esu runs. Between the E $= 173.61$ and E $= 547.2$ esu runs the shift is ~ 0.13°C. The shift is not quadratic in field. We have fitted a linear curve to the experimental data (Figure 3.20). Even in the absence of the electric field the width of the transition temperature is $\sim \pm 0.1$°C. Also, the minimum temperature step is 0.1°C. Taking these experimental limitations into account the data appears to be consistent with a linear variation whereas, according to the Landau theory T_{NI} should depend quadratically on E (see Figure 3.4). Our present measurements are not accurate enough to assert that the dependence is genuinely linear. We have not performed experiments on materials with negative dielectric anisotropy further, as our interest is mainly in studying transitions exhibited by positive dielectric anisotropy.
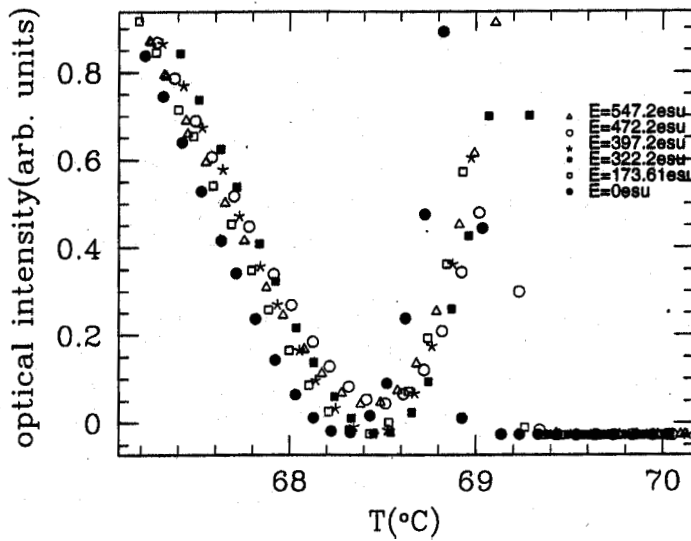
Figure 3.17: Variation of the transmitted optical intensity of a homogeneously aligned S1495 sample as a function of temperature at different fields. The frequency of the applied voltage f=15111 Hz.
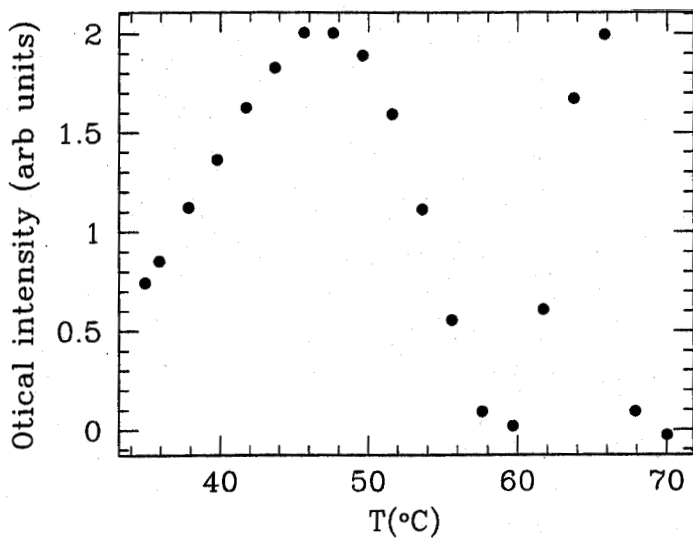

Figure 3.18: Variation of the optical intensity in the nematic phase of S1495 as a function of temperature at $V = 0$.
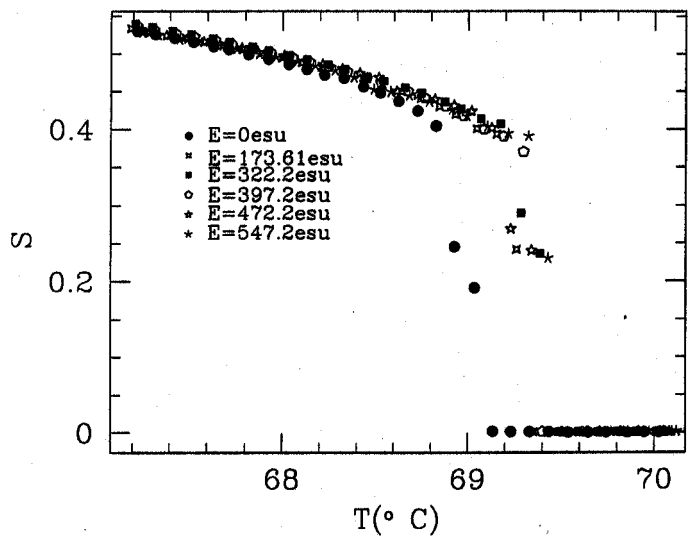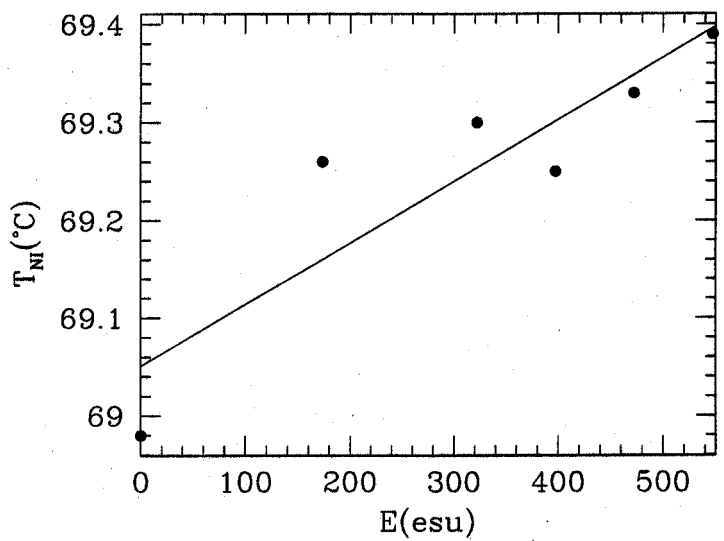
Figure 3.19: Variation of the order parameter of S1495 as a function of temperature at different fields. Calculated from the data shown in Figure 3.17.

Figure, 3.20: Transition temperature temperature of S1495 as a function of field. Taken from the data shown in Figure 3.19.